

Inertial based Integration with Transformed INS Mechanization in Earth Frame

Lubin Chang, Jingbo Di and Fangjun Qin

Abstract—This paper proposes to use a newly-derived transformed inertial navigation system (INS) mechanization to fuse INS with other complimentary sensors. Through formulating the attitude, velocity and position as one group state of group of double direct spatial isometries $\mathbb{SE}_2(3)$, the transformed INS mechanization has proven to be group affine, which opens door to log-linearity and filtering consistency. In order to make use of the transformed INS mechanization in inertial based applications, both the right and left error state models are derived. The INS/GPS and INS/Odometer integration are investigated as two representatives of inertial based applications. Some application aspects of the derived error state models in the two applications are presented, which include how to select the error state model, initialization of the $\mathbb{SE}_2(3)$ based error state covariance and feedback correction corresponding to the error state definitions. Land vehicle experiments are conducted to evaluate the performance of the derived error state models. It is shown that the most striking superiority of using the derived error state models is their ability to handle the large initial attitude misalignments, which is just the result of log-linearity property of the derived error state models. Therefore, the derived error state models can be used in the so-called attitude alignment for the two applications.

Index Terms—Inertial navigation system, transformed INS mechanization, inertial based integration, Lie group, group affine

I. INTRODUCTION

Integrating inertial navigation system (INS) with other complementary sensors is a general and popular strategy for accurate and continuous position and navigation [1-6]. The inertial based integration systems can provide attitude, velocity, position information or parts of these information. The extended Kalman filtering (EKF) has proven to be the workhorse for such inertial based integration applications. However, the EKF may suffer from inconsistency problem in some applications, such as Simultaneous Localization And Mapping (SLAM) and visual-inertial navigation systems (VINS) [7-10]. Such inconsistency problem is mainly caused by the false-observability of some state elements. Some researchers have observed that different state error definitions can lead to different performance [11-16]. With such

The paper was supported in part by National Natural Science Foundation of China (61873275).

The authors are all with the College of Electrical Engineering, Naval University of Engineering. (e-mail: changlubin@163.com, 1452135909@qq.com, haig2005@126.com).

consideration, some researchers make use of alternative state error definitions to circumvent the filtering inconsistency problem [17-22]. Most of these state error definitions fall into the theory of Lie group and Lie algebra. Traditionally, the attitude error is defined on the special orthogonal group $\mathcal{SO}(3)$, while other error state is defined directly in Euclidean space. In [23-25] the group of double direct spatial isometries ($\mathbb{SE}_2(3)$) is introduced to formulate the attitude, velocity and position into a group. With the associated Lie algebra, different velocity and position errors can be derived as opposed to the corresponding errors in Euclidean space. With the state error corresponding to state on $\mathbb{SE}_2(3)$, the linearized error state model is trajectory independent and the filtering inconsistency problem can be remedied naturally for SLAM and VINS.

The trajectory independence of the error state model is rooted in the fact that the group state model satisfies a *group affine* property [23, 26]. Besides the aforementioned ability of remedying the filtering consistency, the *group affine* property also opens door to log-linearity. The log-linearity means that the nonlinear group state error can be recovered exactly from the approximated linear error. Unfortunately, not every group state model satisfies such *group affine* property. It can be deduced from [20, 21] that only when the Earth rotation and Coriolis effect are ignored, the INS mechanization satisfies the *group affine* property. However, for high-precision applications, the Earth rotation and Coriolis effect should be taken into account. This is always the case for INS/GPS and INS/Odometer integration [1, 3, 5]. In order to make use of the striking advantage derived by the *group affine* property, an auxiliary velocity is introduced based on the INS mechanization in Earth-Centered Earth-Fixed Frame (ECEF) [24, 25]. The resultant transformed INS mechanization can now satisfy the *group affine* property. However, the transformed INS mechanization is only used for preintegration on manifolds and the trajectory independent error state model has not been derived. In this paper, we propose to use the transformed INS mechanization for high-precision inertial based integration problem, which necessitates the derivation of the error state model. Through formulating the attitude, transformed velocity and position as an element of $\mathbb{SE}_2(3)$, the error state models corresponding to the transformed INS mechanization with both right and left group error definitions are derived. With INS/GPS and INS/Odometer integration as two representative applications, some application aspects are discussed detailedly

and the performance of the derived error state models in the two applications has also been evaluated comprehensively.

The remaining content is organized as follows. Section II presents the general theory corresponding to INS mechanization in ECEF and Lie group. In Section III, the error state models with both right and left error definitions are derived explicitly. Some application aspects have been discussed in order to facilitate the practical applications of the error state models in Section IV. In Section V land vehicle experiments are conducted to evaluate the performance of the derived error state models for both INS/GPS integration and INS/Odometer integration. Finally, conclusions are drawn in Section VI.

II. PROBLEM FORMULATION

Denote the ECEF as e frame, the inertial frame as i frame and the body frame as b frame. INS mechanization in ECEF frame is given by [27, 28]

$$\begin{aligned}\dot{\mathbf{C}}_b^e &= \mathbf{C}_b^e (\boldsymbol{\omega}_{ib}^b \times) - (\boldsymbol{\omega}_{ie}^e \times) \mathbf{C}_b^e \\ \dot{\mathbf{v}}^e &= \mathbf{C}_b^e \mathbf{f}^b - 2(\boldsymbol{\omega}_{ie}^e \times) \mathbf{v}^e - (\boldsymbol{\omega}_{ie}^e \times)^2 \mathbf{p}^e + \bar{\mathbf{g}}^e \\ \dot{\mathbf{p}}^e &= \mathbf{v}^e\end{aligned}\quad (1)$$

where \mathbf{C}_b^e denotes the direction cosine matrices (DCM) from body frame to ECEF. $\boldsymbol{\omega}_{ib}^b$ is the body angular rate with respect to inertial frame which can be measured by gyroscopes in body frame. $\boldsymbol{\omega}_{ie}^e$ is the Earth rotation rate expressed in the ECEF. $\mathbf{v}^e = [v_x \ v_y \ v_z]^T$ is the ground velocity expressed in ECEF. \mathbf{f}^b is the specific force measured by accelerometers in the body frame. $\mathbf{p}^e = [x \ y \ z]^T$ is the position vector in ECEF. $\bar{\mathbf{g}}^e$ is the gravitational vector and its relationship with the gravity vector \mathbf{g}^e is given by

$$\mathbf{g}^e = \bar{\mathbf{g}}^e - (\boldsymbol{\omega}_{ie}^e \times)^2 \mathbf{p}^e \quad (2)$$

In [22, 23], an auxiliary velocity vector is introduced as

$$\bar{\mathbf{v}}^e = \mathbf{v}^e + (\boldsymbol{\omega}_{ie}^e \times) \mathbf{p}^e \quad (3)$$

With the introduced auxiliary velocity vector, the INS mechanization is now given by

$$\begin{aligned}\dot{\mathbf{C}}_b^e &= \mathbf{C}_b^e (\boldsymbol{\omega}_{ib}^b \times) - (\boldsymbol{\omega}_{ie}^e \times) \mathbf{C}_b^e \\ \dot{\bar{\mathbf{v}}}^e &= \mathbf{C}_b^e \mathbf{f}^b - (\boldsymbol{\omega}_{ie}^e \times) \bar{\mathbf{v}}^e + \bar{\mathbf{g}}^e \\ \dot{\mathbf{p}}^e &= \bar{\mathbf{v}}^e - (\boldsymbol{\omega}_{ie}^e \times) \mathbf{p}^e\end{aligned}\quad (4)$$

Formulating the attitude \mathbf{C}_b^e , velocity $\bar{\mathbf{v}}^e$ and position \mathbf{p}^e as elements of the group of double direct spatial isometries ($\mathcal{SE}_2(3)$)

$$\boldsymbol{\chi} = \begin{bmatrix} \mathbf{C}_b^e & \bar{\mathbf{v}}^e & \mathbf{p}^e \\ \mathbf{0}_{1 \times 3} & 1 & 0 \\ \mathbf{0}_{1 \times 3} & 0 & 1 \end{bmatrix} \quad (5)$$

Eq. (4) can now be rewritten in a compact form as

$$\begin{aligned}\dot{\boldsymbol{\chi}} &= f(\boldsymbol{\chi}) = \\ \begin{bmatrix} \mathbf{C}_b^e (\boldsymbol{\omega}_{ib}^b \times) - (\boldsymbol{\omega}_{ie}^e \times) \mathbf{C}_b^e & \mathbf{C}_b^e \mathbf{f}^b - (\boldsymbol{\omega}_{ie}^e \times) \bar{\mathbf{v}}^e + \bar{\mathbf{g}}^e & \bar{\mathbf{v}}^e - (\boldsymbol{\omega}_{ie}^e \times) \mathbf{p}^e \\ \mathbf{0}_{1 \times 3} & 0 & 0 \\ \mathbf{0}_{1 \times 3} & 0 & 0 \end{bmatrix} \quad (6)\end{aligned}$$

It can be easily verified that dynamic model (6) satisfies the following relationship

$$f(\boldsymbol{\chi}_1 \boldsymbol{\chi}_2) = f(\boldsymbol{\chi}_1) \boldsymbol{\chi}_2 + \boldsymbol{\chi}_1 f(\boldsymbol{\chi}_2) - \boldsymbol{\chi}_1 f(\mathbf{I}_{5 \times 5}) \boldsymbol{\chi}_2 \quad (7)$$

where $\boldsymbol{\chi}_1, \boldsymbol{\chi}_2 \in \mathcal{SE}_2(3)$ are the realizations of the group state (5). One dynamic that satisfies such relationship is regarded as *group affine* dynamic [23]. One striking property of the *group affine* dynamic is that its error state model is independent of the global state, which is very profitable when facing observability problem or large initial misalignment in inertial based applications. In next section, we will derive the explicit error state models with both right and left error definitions.

III. ERROR STATE MODEL

A. Right Error State Model

The right group state error is defined as

$$\begin{aligned}\boldsymbol{\eta}_r &= \boldsymbol{\chi} \tilde{\boldsymbol{\chi}}^{-1} \\ &= \begin{bmatrix} \mathbf{C}_b^e \tilde{\mathbf{C}}_b^{eT} & \bar{\mathbf{v}}^e - \mathbf{C}_b^e \tilde{\mathbf{C}}_b^{eT} \tilde{\bar{\mathbf{v}}}^e & \mathbf{p}^e - \mathbf{C}_b^e \tilde{\mathbf{C}}_b^{eT} \tilde{\mathbf{p}}^e \\ \mathbf{0}_{1 \times 3} & 1 & 0 \\ \mathbf{0}_{1 \times 3} & 0 & 1 \end{bmatrix} \quad (8)\end{aligned}$$

where $\tilde{\mathbf{C}}_b^e$, $\tilde{\bar{\mathbf{v}}}^e$ and $\tilde{\mathbf{p}}^e$ are the error-contaminated navigation parameters provided by INS calculation based on INS mechanization (4).

Denote the attitude error corresponding to $\mathbf{C}_b^e \tilde{\mathbf{C}}_b^{eT}$ in Euler angle form as $\boldsymbol{\varphi}_r$. If $\boldsymbol{\varphi}_r$ assumed to be small value, its relationship with $\mathbf{C}_b^e \tilde{\mathbf{C}}_b^{eT}$ is given by

$$\mathbf{C}_b^e \tilde{\mathbf{C}}_b^{eT} \approx \mathbf{I}_{3 \times 3} + (\boldsymbol{\varphi}_r \times) \quad (9)$$

With approximation (9), the nonlinear velocity and position errors in (8) can be approximated as

$$\begin{aligned}\mathbf{d}\bar{\mathbf{v}}_r &= \bar{\mathbf{v}}^e - \mathbf{C}_b^e \tilde{\mathbf{C}}_b^{eT} \tilde{\bar{\mathbf{v}}}^e \\ &\approx \bar{\mathbf{v}}^e - [\mathbf{I}_{3 \times 3} + (\boldsymbol{\varphi}_r \times)] \tilde{\bar{\mathbf{v}}}^e = (\tilde{\bar{\mathbf{v}}}^e \times) \boldsymbol{\varphi}_r - \delta \bar{\mathbf{v}}^e\end{aligned}\quad (10)$$

$$\begin{aligned}\mathbf{d}\mathbf{p}_r &= \mathbf{p}^e - \mathbf{C}_b^e \tilde{\mathbf{C}}_b^{eT} \tilde{\mathbf{p}}^e \\ &\approx \mathbf{p}^e - [\mathbf{I}_{3 \times 3} + (\boldsymbol{\varphi}_r \times)] \tilde{\mathbf{p}}^e = (\tilde{\mathbf{p}}^e \times) \boldsymbol{\varphi}_r - \delta \mathbf{p}^e\end{aligned}\quad (11)$$

where $\delta \bar{\mathbf{v}}^e = \tilde{\bar{\mathbf{v}}}^e - \bar{\mathbf{v}}^e$ and $\delta \mathbf{p}^e = \tilde{\mathbf{p}}^e - \mathbf{p}^e$.

According to (4), we can easily derive the error model for $\boldsymbol{\varphi}_r$, $\delta \bar{\mathbf{v}}^e$ and $\delta \mathbf{p}^e$ as

$$\dot{\boldsymbol{\varphi}}_r = -(\boldsymbol{\omega}_{ie}^e \times) \boldsymbol{\varphi}_r - \tilde{\mathbf{C}}_b^e \delta \boldsymbol{\omega}_{ib}^b \quad (12a)$$

$$\dot{\delta \bar{\mathbf{v}}}^e = (\tilde{\mathbf{C}}_b^e \tilde{\mathbf{f}}^b \times) \boldsymbol{\varphi}_r - (\boldsymbol{\omega}_{ie}^e \times) \delta \bar{\mathbf{v}}^e + \tilde{\mathbf{C}}_b^e \delta \mathbf{f}^b \quad (12b)$$

$$\dot{\delta \mathbf{p}}^e = \delta \bar{\mathbf{v}}^e - (\boldsymbol{\omega}_{ie}^e \times) \delta \mathbf{p}^e \quad (12c)$$

where $\delta \boldsymbol{\omega}_{ib}^b = \tilde{\boldsymbol{\omega}}_{ib}^b - \boldsymbol{\omega}_{ib}^b$ with $\tilde{\boldsymbol{\omega}}_{ib}^b$ be measured by gyroscopes and $\delta \mathbf{f}^b = \tilde{\mathbf{f}}^b - \mathbf{f}^b$ with $\tilde{\mathbf{f}}^b$ be measured by accelerometers. When deriving (12b), $\bar{\mathbf{g}}^e$ has been assumed to be an error-free

constant although it is also a function of the position. The error state $[\boldsymbol{\varphi}_r^T \ \boldsymbol{\delta\bar{v}}^T \ \boldsymbol{\delta\bar{p}}^T]^T$ can be viewed as definition on $\mathcal{SO}(3) + \mathbb{R}^6$ in contrast with the error state $[\boldsymbol{\varphi}_r^T \ \boldsymbol{d\bar{v}}_r^T \ \boldsymbol{d\bar{p}}_r^T]^T$ defined on $\mathcal{SE}_2(3)$.

With definitions (10) and (11) and the error state model (12), we now derive the differential equations of $\boldsymbol{d\bar{v}}_r$ and $\boldsymbol{d\bar{p}}_r$ as follows.

Taking differential operation on both sides of (10) gives

$$\dot{\boldsymbol{d\bar{v}}}_r = (\dot{\tilde{\mathbf{v}}}^e \times) \boldsymbol{\varphi}_r + (\tilde{\mathbf{v}}^e \times) \dot{\boldsymbol{\varphi}}_r - \boldsymbol{\delta\bar{v}}^e \quad (13)$$

Substituting (4) and (12) into (13) gives

$$\begin{aligned} \dot{\boldsymbol{d\bar{v}}}_r &= \left[\tilde{\mathbf{C}}_b^e \tilde{\mathbf{f}}^b - (\boldsymbol{\omega}_{ie}^e \times) \tilde{\mathbf{v}}^e + \tilde{\mathbf{g}}^e \right] \times \boldsymbol{\varphi}_r + (\tilde{\mathbf{v}}^e \times) \left[-(\boldsymbol{\omega}_{ie}^e \times) \boldsymbol{\varphi}_r - \tilde{\mathbf{C}}_b^e \boldsymbol{\delta\omega}_{ib}^b \right] \\ &\quad - \left[(\tilde{\mathbf{C}}_b^e \tilde{\mathbf{f}}^b \times) \boldsymbol{\varphi}_r - (\boldsymbol{\omega}_{ie}^e \times) \boldsymbol{\delta\bar{v}}^e + \tilde{\mathbf{C}}_b^e \boldsymbol{\delta\bar{f}}^b \right] \\ &= \left[(\tilde{\mathbf{g}}^e \times) - (\boldsymbol{\omega}_{ie}^e \times) (\tilde{\mathbf{v}}^e \times) \right] \boldsymbol{\varphi}_r + (\boldsymbol{\omega}_{ie}^e \times) \boldsymbol{\delta\bar{v}}^e - (\tilde{\mathbf{v}}^e \times) \tilde{\mathbf{C}}_b^e \boldsymbol{\delta\omega}_{ib}^b - \tilde{\mathbf{C}}_b^e \boldsymbol{\delta\bar{f}}^b \\ &= \left[(\tilde{\mathbf{g}}^e \times) - (\boldsymbol{\omega}_{ie}^e \times) (\tilde{\mathbf{v}}^e \times) \right] \boldsymbol{\varphi}_r + (\boldsymbol{\omega}_{ie}^e \times) \left[(\tilde{\mathbf{v}}^e \times) \boldsymbol{\varphi}_r - \boldsymbol{d\bar{v}}_r \right] \\ &\quad - (\tilde{\mathbf{v}}^e \times) \tilde{\mathbf{C}}_b^e \boldsymbol{\delta\omega}_{ib}^b - \tilde{\mathbf{C}}_b^e \boldsymbol{\delta\bar{f}}^b \\ &= (\tilde{\mathbf{g}}^e \times) \boldsymbol{\varphi}_r - (\boldsymbol{\omega}_{ie}^e \times) \boldsymbol{d\bar{v}}_r - (\tilde{\mathbf{v}}^e \times) \tilde{\mathbf{C}}_b^e \boldsymbol{\delta\omega}_{ib}^b - \tilde{\mathbf{C}}_b^e \boldsymbol{\delta\bar{f}}^b \end{aligned} \quad (14)$$

Taking differential operation on both sides of (11) gives

$$\dot{\boldsymbol{d\bar{p}}}_r = (\dot{\tilde{\mathbf{p}}}^e \times) \boldsymbol{\varphi}_r + (\tilde{\mathbf{p}}^e \times) \dot{\boldsymbol{\varphi}}_r - \boldsymbol{\delta\bar{p}}^e \quad (15)$$

Substituting (4) and (12) into (15) gives

$$\begin{aligned} \dot{\boldsymbol{d\bar{p}}}_r &= \left[\tilde{\mathbf{v}}^e - (\boldsymbol{\omega}_{ie}^e \times) \boldsymbol{p}^e \right] \times \boldsymbol{\varphi}_r + (\tilde{\mathbf{p}}^e \times) \left[-(\boldsymbol{\omega}_{ie}^e \times) \boldsymbol{\varphi}_r - \tilde{\mathbf{C}}_b^e \boldsymbol{\delta\omega}_{ib}^b \right] \\ &\quad - \left[\boldsymbol{\delta\bar{v}}^e - (\boldsymbol{\omega}_{ie}^e \times) \boldsymbol{\delta\bar{p}}^e \right] \\ &= \left[\tilde{\mathbf{v}}^e - (\boldsymbol{\omega}_{ie}^e \times) \boldsymbol{p}^e \right] \times \boldsymbol{\varphi}_r + (\tilde{\mathbf{p}}^e \times) \left[-(\boldsymbol{\omega}_{ie}^e \times) \boldsymbol{\varphi}_r - \tilde{\mathbf{C}}_b^e \boldsymbol{\delta\omega}_{ib}^b \right] \\ &\quad - \left[(\tilde{\mathbf{v}}^e \times) \boldsymbol{\varphi}_r - \boldsymbol{d\bar{v}}_r - (\boldsymbol{\omega}_{ie}^e \times) \left[(\tilde{\mathbf{p}}^e \times) \boldsymbol{\varphi}_r - \boldsymbol{\delta\bar{p}}_r \right] \right] \\ &= -\boldsymbol{d\bar{v}}_r + (\boldsymbol{\omega}_{ie}^e \times) \boldsymbol{d\bar{p}}_r - (\tilde{\mathbf{p}}^e \times) \tilde{\mathbf{C}}_b^e \boldsymbol{\delta\omega}_{ib}^b \end{aligned} \quad (16)$$

For the inertial sensors, if we only consider the drift bias and noise, $\boldsymbol{\delta\omega}_{ib}^b$ and $\boldsymbol{\delta\bar{f}}^b$ can be given by

$$\boldsymbol{\delta\omega}_{ib}^b = \boldsymbol{\varepsilon}^b + \boldsymbol{\eta}_g^b \quad (17a)$$

$$\boldsymbol{\delta\bar{f}}^b = \boldsymbol{\nabla}^b + \boldsymbol{\eta}_a^b \quad (17b)$$

where $\boldsymbol{\varepsilon}^b$ is gyroscope drift bias and $\boldsymbol{\eta}_g^b$ the corresponding noise.

$\boldsymbol{\nabla}^b$ is accelerometer drift bias and $\boldsymbol{\eta}_a^b$ the corresponding noise.

Define the state vector as

$$\boldsymbol{dx}_r = [\boldsymbol{\varphi}_r \ \boldsymbol{d\bar{v}}_r \ \boldsymbol{d\bar{p}}_r \ \boldsymbol{\varepsilon}^b \ \boldsymbol{\nabla}^b]^T \quad (18)$$

The corresponding state space model is given by

$$\dot{\boldsymbol{dx}}_r = \mathbf{F}_r \boldsymbol{dx}_r + \mathbf{G}_r \begin{bmatrix} \boldsymbol{\eta}_g^b \\ \boldsymbol{\eta}_a^b \end{bmatrix} \quad (19a)$$

where

$$\mathbf{F}_r = \begin{bmatrix} -(\boldsymbol{\omega}_{ie}^e \times) & \mathbf{0}_{3 \times 3} & \mathbf{0}_{3 \times 3} & -\tilde{\mathbf{C}}_b^e & \mathbf{0}_{3 \times 3} \\ (\tilde{\mathbf{g}}^e \times) & -(\boldsymbol{\omega}_{ie}^e \times) & \mathbf{0}_{3 \times 3} & -(\tilde{\mathbf{v}}^e \times) \tilde{\mathbf{C}}_b^e & -\tilde{\mathbf{C}}_b^e \\ \mathbf{0}_{3 \times 3} & \mathbf{I}_{3 \times 3} & -(\boldsymbol{\omega}_{ie}^e \times) & -(\tilde{\mathbf{p}}^e \times) \tilde{\mathbf{C}}_b^e & \mathbf{0}_{3 \times 3} \\ \mathbf{0}_{3 \times 3} & \mathbf{0}_{3 \times 3} & \mathbf{0}_{3 \times 3} & \mathbf{0}_{3 \times 3} & \mathbf{0}_{3 \times 3} \\ \mathbf{0}_{3 \times 3} & \mathbf{0}_{3 \times 3} & \mathbf{0}_{3 \times 3} & \mathbf{0}_{3 \times 3} & \mathbf{0}_{3 \times 3} \end{bmatrix} \quad (19b)$$

$$\mathbf{G}_r = \begin{bmatrix} -\tilde{\mathbf{C}}_b^e & \mathbf{0}_{3 \times 3} \\ -(\tilde{\mathbf{v}}^e \times) \tilde{\mathbf{C}}_b^e & -\tilde{\mathbf{C}}_b^e \\ -(\tilde{\mathbf{p}}^e \times) \tilde{\mathbf{C}}_b^e & \mathbf{0}_{3 \times 3} \\ \mathbf{0}_{3 \times 3} & \mathbf{0}_{3 \times 3} \\ \mathbf{0}_{3 \times 3} & \mathbf{0}_{3 \times 3} \end{bmatrix} \quad (19c)$$

It is shown that if we do not consider inertial sensors' error, the state transition matrix is independent of the global state. This is just striking result of the *group affine* property. The trajectory independent linearized model on one hand can handle the filtering inconsistency caused by false-observability of certain state element. This has been widely investigated in field of SLAM and VINS. On the other hand, it opens the door to *log-linearity* in Kalman filtering. The *log-linearity* is not the typical Jacobian linearization along a trajectory because the nonlinear error on the group can be exactly recovered from its solution. Such conclusion is very profitable for attitude alignment with arbitrary misalignments [29-32]. Although incorporating the drift biases into the error state will cause state-dependence for the resultant augmented state transition matrix, much of the benefit provided by the *log-linearity* can be reserved [26]. That is to say, it is still possible to obtain performance improvement making use of the model (19) compared with traditional error state model.

B. Left Error State Model

The left group state error is defined as

$$\begin{aligned} \boldsymbol{\eta}_l &= \tilde{\mathbf{C}}_b^e \boldsymbol{\chi} \\ &= \begin{bmatrix} \tilde{\mathbf{C}}_b^{eT} \tilde{\mathbf{C}}_b^e & \tilde{\mathbf{C}}_b^{eT} (\tilde{\mathbf{v}}^e - \tilde{\mathbf{v}}^e) & \tilde{\mathbf{C}}_b^{eT} (\boldsymbol{p}^e - \tilde{\mathbf{p}}^e) \\ \mathbf{0}_{1 \times 3} & 1 & 0 \\ \mathbf{0}_{1 \times 3} & 0 & 1 \end{bmatrix} \end{aligned} \quad (20)$$

Denote the attitude error corresponding to $\tilde{\mathbf{C}}_b^e \boldsymbol{\chi}$ in Euler angle form as $\boldsymbol{\varphi}_l$. If $\boldsymbol{\varphi}_l$ assumed to be small value, its relationship with $\tilde{\mathbf{C}}_b^{eT} \tilde{\mathbf{C}}_b^e$ is given by

$$\tilde{\mathbf{C}}_b^{eT} \tilde{\mathbf{C}}_b^e \approx \mathbf{I}_{3 \times 3} + (\boldsymbol{\varphi}_l \times) \quad (21)$$

The differential equation of $\boldsymbol{\varphi}_l$ is given by

$$\dot{\boldsymbol{\varphi}}_l = -(\tilde{\boldsymbol{\omega}}_{ib}^b \times) \boldsymbol{\varphi}_l - \boldsymbol{\delta\omega}_{ib}^b \quad (22)$$

With approximation (21), the velocity and position errors in (20) can be approximated as

$$\boldsymbol{d\bar{v}}_l \approx \tilde{\mathbf{C}}_b^{eT} (\tilde{\mathbf{v}}^e - \tilde{\mathbf{v}}^e) = -\tilde{\mathbf{C}}_b^{eT} \boldsymbol{\delta\bar{v}}^e \quad (23)$$

$$\boldsymbol{d\bar{p}}_l \approx \tilde{\mathbf{C}}_b^{eT} (\boldsymbol{p}^e - \tilde{\mathbf{p}}^e) = -\tilde{\mathbf{C}}_b^{eT} \boldsymbol{\delta\bar{p}}^e \quad (24)$$

Taking differential operation on both sides of (23) gives

$$\dot{\mathbf{d}\bar{v}}_l = -\tilde{\mathbf{C}}_b^{eT} \dot{\mathbf{\delta v}}^e - \dot{\tilde{\mathbf{C}}}_b^{eT} \dot{\mathbf{\delta v}}^e \quad (25)$$

Substituting (4) and (12) into (25) gives

$$\begin{aligned} \dot{\mathbf{d}\bar{v}}_l &= -\tilde{\mathbf{C}}_b^{eT} \left[\left(\tilde{\mathbf{C}}_b^e \tilde{\mathbf{f}}^b \times \right) \mathbf{\Phi}_l - \left(\mathbf{\omega}_{ie}^e \times \right) \mathbf{\delta v}^e + \tilde{\mathbf{C}}_b^e \mathbf{\delta f}^b \right] \\ &\quad - \left[\tilde{\mathbf{C}}_b^e \left(\tilde{\mathbf{\omega}}_{ib}^b \times \right) - \left(\mathbf{\omega}_{ie}^e \times \right) \tilde{\mathbf{C}}_b^e \right]^T \mathbf{\delta v}^e \\ &= -\left(\tilde{\mathbf{f}}^b \times \right) \mathbf{\Phi}_l + \tilde{\mathbf{C}}_b^{eT} \left(\mathbf{\omega}_{ie}^e \times \right) \mathbf{\delta v}^e - \mathbf{\delta f}^b \\ &\quad + \left(\tilde{\mathbf{\omega}}_{ib}^b \times \right) \tilde{\mathbf{C}}_b^{eT} \mathbf{\delta v}^e - \tilde{\mathbf{C}}_b^{eT} \left(\mathbf{\omega}_{ie}^e \times \right) \mathbf{\delta v}^e \\ &= -\left(\tilde{\mathbf{f}}^b \times \right) \mathbf{\Phi}_l - \left(\tilde{\mathbf{\omega}}_{ib}^b \times \right) \mathbf{d\bar{v}}_l - \mathbf{\delta p}^b \end{aligned} \quad (26)$$

It should be noted that in (12b), the attitude error is denoted as $\mathbf{\Phi}_r$. When the attitude error is defined as in (21), the corresponding velocity error model is with the same form as (12b) and the only difference is that $\mathbf{\Phi}_r$ is substituted by $\mathbf{\Phi}_l$.

Taking differential operation on both sides of (24) gives

$$\dot{\mathbf{d}\bar{p}}_l = -\tilde{\mathbf{C}}_b^{eT} \mathbf{\delta p}^e - \tilde{\mathbf{C}}_b^{eT} \mathbf{\delta p}^e \quad (27)$$

Substituting (4) and (12) into (27) gives

$$\begin{aligned} \dot{\mathbf{d}\bar{p}}_l &= -\tilde{\mathbf{C}}_b^{eT} \left[\mathbf{\delta v}^e - \left(\mathbf{\omega}_{ie}^e \times \right) \mathbf{\delta p}^e \right] - \left[\tilde{\mathbf{C}}_b^e \left(\tilde{\mathbf{\omega}}_{ib}^b \times \right) - \left(\mathbf{\omega}_{ie}^e \times \right) \tilde{\mathbf{C}}_b^e \right]^T \mathbf{\delta p}^e \\ &= \mathbf{d\bar{v}}_l + \tilde{\mathbf{C}}_b^{eT} \left(\mathbf{\omega}_{ie}^e \times \right) \mathbf{\delta p}^e + \left(\tilde{\mathbf{\omega}}_{ib}^b \times \right) \tilde{\mathbf{C}}_b^{eT} \mathbf{\delta p}^e - \tilde{\mathbf{C}}_b^{eT} \left(\mathbf{\omega}_{ie}^e \times \right) \mathbf{\delta p}^e \\ &= \mathbf{d\bar{v}}_l - \left(\tilde{\mathbf{\omega}}_{ib}^b \times \right) \mathbf{d\bar{p}}_l \end{aligned} \quad (28)$$

Define the state vector as

$$\mathbf{dx}_l = \left[\mathbf{\Phi}_l \quad \mathbf{d\bar{v}}_l \quad \mathbf{d\bar{p}}_l \quad \mathbf{\varepsilon}^b \quad \nabla^b \right]^T \quad (29)$$

The corresponding state space model is given by

$$\dot{\mathbf{dx}}_l = \mathbf{F}_l \mathbf{dx}_l + \mathbf{G}_l \begin{bmatrix} \mathbf{\eta}_g^b \\ \mathbf{\eta}_a^b \end{bmatrix} \quad (30a)$$

where

$$\mathbf{F}_l = \begin{bmatrix} -\left(\tilde{\mathbf{\omega}}_{ib}^b \times \right) & \mathbf{0}_{3 \times 3} & \mathbf{0}_{3 \times 3} & -\mathbf{I}_{3 \times 3} & \mathbf{0}_{3 \times 3} \\ -\left(\tilde{\mathbf{f}}^b \times \right) & -\left(\tilde{\mathbf{\omega}}_{ib}^b \times \right) & \mathbf{0}_{3 \times 3} & \mathbf{0}_{3 \times 3} & -\mathbf{I}_{3 \times 3} \\ \mathbf{0}_{3 \times 3} & \mathbf{I}_{3 \times 3} & -\left(\tilde{\mathbf{\omega}}_{ib}^b \times \right) & \mathbf{0}_{3 \times 3} & \mathbf{0}_{3 \times 3} \\ \mathbf{0}_{3 \times 3} & \mathbf{0}_{3 \times 3} & \mathbf{0}_{3 \times 3} & \mathbf{0}_{3 \times 3} & \mathbf{0}_{3 \times 3} \\ \mathbf{0}_{3 \times 3} & \mathbf{0}_{3 \times 3} & \mathbf{0}_{3 \times 3} & \mathbf{0}_{3 \times 3} & \mathbf{0}_{3 \times 3} \end{bmatrix} \quad (30b)$$

$$\mathbf{G}_l = \begin{bmatrix} -\mathbf{I}_{3 \times 3} & \mathbf{0}_{3 \times 3} \\ \mathbf{0}_{3 \times 3} & -\mathbf{I}_{3 \times 3} \\ \mathbf{0}_{3 \times 3} & \mathbf{0}_{3 \times 3} \\ \mathbf{0}_{3 \times 3} & \mathbf{0}_{3 \times 3} \\ \mathbf{0}_{3 \times 3} & \mathbf{0}_{3 \times 3} \end{bmatrix} \quad (30c)$$

Interestingly, for the left error definition, the state transition matrix is still independent of the global state even when incorporating the inertial sensors' error into the state.

IV. APPLICATION ASPECTS

A. Error State Model Selection

It is known from last section that there are two different error state definitions and corresponding error state models. How to select the error state model in practical application can be

determined according to the invariant type of the observations. The invariant observations are defined as [23, 26]

$$\text{Left-Invariant Observation: } \mathbf{y} = \chi \mathbf{b} \quad (31a)$$

$$\text{Right-Invariant Observation: } \mathbf{y} = \chi^{-1} \mathbf{b} \quad (31b)$$

where \mathbf{b} is a constant vector. If one observation satisfies (31), the resultant linearized observation model will also be autonomous. More specifically, if the observation is left-invariant, with the left error definition the linearized observation model will be independent of the global state. Similarly, if the observation is right-invariant, with the right error definition the linearized observation model will be independent of the global state.

In this section, we consider two typical applications, that is, INS/GPS integration and INS/Odometer integration. For INS/GPS integration, the GPS can provide accurate velocity and position. Therefore, the observation can be given by

$$\mathbf{y}_{\text{GPS}} = \mathbf{v}_{\text{GPS}}^e + \left(\mathbf{\omega}_{ie}^e \times \right) \mathbf{p}_{\text{GPS}}^e \quad (32)$$

It can be easily verified that the observation in (32) is a left-invariant observation with the group state (5). In this paper, the linearized state-space model is used in the indirect integration. With the left error definition (29), the observation transition function is given by

$$\mathbf{z}_{\text{obser}} = \underbrace{\begin{bmatrix} \mathbf{0}_{3 \times 3} & -\tilde{\mathbf{C}}_b^e & \mathbf{0}_{3 \times 9} \end{bmatrix}}_{\mathbf{H}_l} \mathbf{dx}_l \quad (33)$$

where

$$\mathbf{z}_{\text{obser}} = \tilde{\mathbf{v}}^e - \mathbf{y}_{\text{GPS}} \quad (34)$$

It seems that the transition matrix in (33) is dependent on the global state $\tilde{\mathbf{C}}_b^e$. Actually, as pointed out in [22] that “*Applying a linear function to the innovation term of an EKF before computing the gains does not change the results of the filter*”. Therefore, we can construct a transformed observation and the corresponding transition matrix as

$$\bar{\mathbf{z}}_{\text{obser}} = \tilde{\mathbf{C}}_b^{eT} \mathbf{z}_{\text{obser}} \quad (35)$$

$$\bar{\mathbf{H}}_l = \tilde{\mathbf{C}}_b^{eT} \mathbf{H}_l = \left[\mathbf{0}_{3 \times 3} \quad -\mathbf{I}_{3 \times 3} \quad \mathbf{0}_{3 \times 9} \right] \quad (36)$$

Now, it is clearly shown that $\bar{\mathbf{H}}_l$ is no longer dependent on the global state.

Similarly, if the position vector $\mathbf{p}_{\text{GPS}}^e$ is used directly, it can be verified that it is also a left-invariant observation. However, if the velocity $\mathbf{v}_{\text{GPS}}^e$ is used directly, it can be verified that $\mathbf{v}_{\text{GPS}}^e$ is neither left-invariant nor right-invariant. In this case, with left error definition the indirect observation is given by

$$\begin{aligned} \mathbf{z}_{\text{obser}} &= \tilde{\mathbf{v}}^e - \mathbf{v}_{\text{GPS}}^e = \tilde{\mathbf{v}}^e - \left(\mathbf{\omega}_{ie}^e \times \right) \tilde{\mathbf{p}}^e - \mathbf{v}_{\text{GPS}}^e \\ &= \mathbf{\delta v}^e = \mathbf{\delta v}^e - \left(\mathbf{\omega}_{ie}^e \times \right) \mathbf{\delta p}^e \\ &= -\tilde{\mathbf{C}}_b^e \mathbf{d\bar{v}}^e + \left(\mathbf{\omega}_{ie}^e \times \right) \tilde{\mathbf{C}}_b^e \mathbf{d\bar{p}}^e \end{aligned} \quad (37)$$

It is shown that the transition matrix derived from (37) is dependent on the global state $\tilde{\mathbf{C}}_b^e$ and we cannot left-multiply $\tilde{\mathbf{C}}_b^{eT}$ to remove such dependence. However, $\mathbf{v}_{\text{GPS}}^e$ is *more like* left-invariant, it is still appropriate to apply the left error definition.

For INS/Odometer integration, the observation is the body velocity \mathbf{v}^b . With the group state (5), it can be verified that \mathbf{v}^b is neither left-invariant nor right-invariant. However, if we consider the group state

$$\boldsymbol{\gamma} = \begin{bmatrix} \mathbf{C}_b^e & \mathbf{v}^e & \mathbf{p}^e \\ \mathbf{0}_{1 \times 3} & 1 & 0 \\ \mathbf{0}_{1 \times 3} & 0 & 1 \end{bmatrix} \quad (38)$$

It can be verified that

$$\mathbf{v}^b = \boldsymbol{\gamma}^{-1} \mathbf{b} = \begin{bmatrix} \mathbf{C}_b^{eT} & -\mathbf{C}_b^{eT} \mathbf{v}^e & -\mathbf{C}_b^{eT} \mathbf{p}^e \\ \mathbf{0}_{1 \times 3} & 1 & 0 \\ \mathbf{0}_{1 \times 3} & 0 & 1 \end{bmatrix} \begin{bmatrix} 0 \\ -1 \\ 0 \end{bmatrix} \quad (39)$$

That is to say, \mathbf{v}^b is right-invariant for the group state (38). In this respect, we can say that \mathbf{v}^b is *more like* right-invariant for the group state (5). Therefore, it is still appropriate to apply the right error definition. With right error definition, the indirect observation is given by

$$\begin{aligned} \mathbf{y} &= \tilde{\mathbf{v}}^e - (\boldsymbol{\omega}_{ie}^e \times) \tilde{\mathbf{p}}^e - \tilde{\mathbf{C}}_b^e \mathbf{v}^b \\ &= \tilde{\mathbf{v}}^e - \tilde{\mathbf{C}}_b^e \mathbf{v}^b = -(\mathbf{v}^e \times) \boldsymbol{\phi}_r + \boldsymbol{\delta v}^e \\ &= -[\tilde{\mathbf{v}}^e - (\boldsymbol{\omega}_{ie}^e \times) \mathbf{p}^e] \times \boldsymbol{\phi}_r + \boldsymbol{\delta \bar{v}}^e - (\boldsymbol{\omega}_{ie}^e \times) \boldsymbol{\delta p}^e \\ &= [-(\tilde{\mathbf{v}}^e \times) + (\boldsymbol{\omega}_{ie}^e \times) (\mathbf{p}^e \times) - (\mathbf{p}^e \times) (\boldsymbol{\omega}_{ie}^e \times)] \boldsymbol{\phi}_r \\ &\quad + \boldsymbol{\delta \bar{v}}^e + (\tilde{\mathbf{v}}^e \times) \boldsymbol{\phi}_r - (\boldsymbol{\omega}_{ie}^e \times) \boldsymbol{\delta p}^e \\ &= [(\boldsymbol{\omega}_{ie}^e \times) (\mathbf{p}^e \times) - (\mathbf{p}^e \times) (\boldsymbol{\omega}_{ie}^e \times)] \boldsymbol{\phi}_r + \boldsymbol{\delta \bar{v}}^e - (\boldsymbol{\omega}_{ie}^e \times) \boldsymbol{\delta p}^e \\ &= [(\boldsymbol{\omega}_{ie}^e \times) (\mathbf{p}^e \times) - (\mathbf{p}^e \times) (\boldsymbol{\omega}_{ie}^e \times)] \boldsymbol{\phi}_r + \boldsymbol{\delta \bar{v}}^e \\ &\quad - (\boldsymbol{\omega}_{ie}^e \times) [\boldsymbol{\delta p}^e + (\mathbf{p}^e \times) \boldsymbol{\phi}_r] \\ &\approx [-(\tilde{\mathbf{p}}^e \times) (\boldsymbol{\omega}_{ie}^e \times)] \boldsymbol{\phi}_r + \boldsymbol{\delta \bar{v}}^e - (\boldsymbol{\omega}_{ie}^e \times) \boldsymbol{\delta p}^e \end{aligned} \quad (40)$$

It is shown that the transition matrix derived from (40) is dependent on the global state $\tilde{\mathbf{p}}^e$.

B. Initial Covariance Setting

The initial covariance setting can affect the filtering performance. Generally, if the state vector is not correlated with each other, the diagonal elements of the covariance can be given empirically according to the pre-knowledge degree of these values. However, for the correlated state defined in this paper, the covariance cannot be set so directly based on the experience. If we have set an initial covariance $\mathbf{P}_{\text{avp},0}$ for the error state $[\boldsymbol{\phi}^T \ \boldsymbol{\delta v}^{eT} \ \boldsymbol{\delta p}^{eT}]^T$ empirically, the initial covariance $\mathbf{P}_{\text{avp},r0}$ for the right error state $[\boldsymbol{\phi}_r^T \ \boldsymbol{\delta \bar{v}}_r^T \ \boldsymbol{\delta p}_r^T]^T$ can be determined according to the transformation (3), (10) and (11) as

$$\mathbf{P}_{\text{avp},r0} = \mathbf{T}_R \mathbf{P}_{\text{avp},0} \mathbf{T}_R^T \quad (41)$$

where

$$\mathbf{T}_R = \begin{bmatrix} \mathbf{I}_{3 \times 3} & \mathbf{0}_{3 \times 3} & \mathbf{0}_{3 \times 3} \\ (\tilde{\mathbf{v}}_0^e \times) & -\mathbf{I}_{3 \times 3} & (\boldsymbol{\omega}_{ie}^e \times) \\ (\tilde{\mathbf{p}}_0^e \times) & \mathbf{0}_{3 \times 3} & -\mathbf{I}_{3 \times 3} \end{bmatrix} \quad (42)$$

where $\tilde{\mathbf{v}}_0^e$ is the initial velocity and $\tilde{\mathbf{p}}_0^e$ is the initial position.

The initial covariance $\mathbf{P}_{\text{avp},l0}$ for the left error state $[\boldsymbol{\phi}_l^T \ \boldsymbol{\delta \bar{v}}_l^T \ \boldsymbol{\delta p}_l^T]^T$ can be determined according to the transformation (3), (23) and (24) as

$$\mathbf{P}_{\text{avp},l0} = \mathbf{T}_L \mathbf{P}_{\text{avp},0} \mathbf{T}_L^T \quad (43)$$

where

$$\mathbf{T}_L = \begin{bmatrix} \mathbf{I}_{3 \times 3} & \mathbf{0}_{3 \times 3} & \mathbf{0}_{3 \times 3} \\ \mathbf{0}_{3 \times 3} & -\tilde{\mathbf{C}}_{b,0}^{eT} & -\tilde{\mathbf{C}}_{b,0}^{eT} (\boldsymbol{\omega}_{ie}^e \times) \\ \mathbf{0}_{3 \times 3} & \mathbf{0}_{3 \times 3} & -\tilde{\mathbf{C}}_{b,0}^{eT} \end{bmatrix} \quad (44)$$

where $\tilde{\mathbf{C}}_{b,0}^e$ is the initial attitude matrix.

C. Feedback Correction

There are three sequential stages for the indirect integration at one time instant, i.e. INS calculation, Kalman filtering and feedback correction. The Kalman filtering is virtually used to estimate the error state as defined in (18) or (29). After the Kalman filtering, the estimated error state is used to refine the INS calculation result, which is just the feedback correction. The feedback correction is corresponding to the error state definition and can be viewed as the inverse operation. For the right error definition, the feedback correction at time instant k is given by

$$\hat{\mathbf{C}}_{b,k}^n = \exp(\hat{\boldsymbol{\phi}}_{r,k}) \tilde{\mathbf{C}}_{b,k}^n \quad (45a)$$

$$\hat{\mathbf{v}}_k^e = \tilde{\mathbf{v}}_k^e + \mathbf{d}\hat{\mathbf{v}}_{r,k} - \tilde{\mathbf{v}}_k^e \times \hat{\boldsymbol{\phi}}_{r,k} \quad (45b)$$

$$\hat{\mathbf{p}}_k^e = \tilde{\mathbf{p}}_k^e + \mathbf{d}\hat{\mathbf{p}}_{r,k} - \tilde{\mathbf{p}}_k^e \times \hat{\boldsymbol{\phi}}_{r,k} \quad (45c)$$

where $\tilde{\mathbf{C}}_{b,k}^n$, $\tilde{\mathbf{v}}_k^e$ and $\tilde{\mathbf{p}}_k^e$ are the INS calculation result. $\hat{\boldsymbol{\phi}}_{r,k}$, $\mathbf{d}\hat{\mathbf{v}}_{r,k}$ and $\mathbf{d}\hat{\mathbf{p}}_{r,k}$ are the error state estimate by the Kalman filtering.

$\hat{\mathbf{C}}_{b,k}^n$, $\hat{\mathbf{v}}_k^e$ and $\hat{\mathbf{p}}_k^e$ are the refined navigation parameters and will be used as inputs for INS to calculate $\tilde{\mathbf{C}}_{b,k+1}^n$, $\tilde{\mathbf{v}}_{k+1}^e$ and $\tilde{\mathbf{p}}_{k+1}^e$ at next time instant.

Similarly, for the left error definition, the feedback correction at time instant k is given by

$$\hat{\mathbf{C}}_{b,k}^e = \tilde{\mathbf{C}}_{b,k}^e \exp(\hat{\boldsymbol{\phi}}_{l,k}) \quad (46a)$$

$$\hat{\mathbf{v}}_k^e = \tilde{\mathbf{C}}_{b,k}^e \mathbf{d}\hat{\mathbf{v}}_{l,k} + \hat{\mathbf{v}}_k^e \quad (46b)$$

$$\hat{\mathbf{p}}_k^e = \tilde{\mathbf{C}}_{b,k}^e \mathbf{d}\hat{\mathbf{p}}_{l,k} + \tilde{\mathbf{p}}_k^e \quad (46c)$$

After the state update, the corresponding error state estimate should be reset to zero, that is $\mathbf{d}\hat{\mathbf{x}}_{r/l,k}(1:9) = \mathbf{0}_{9 \times 1}$. (45) and (46) are only used to refine the global state. There is no consensus yet about that is it necessary to update the covariance corresponding to the state update (45) and (46) [33]. In this paper, we adopt the statement that the reset operation does not provide new information and will not perform covariance update for the global state update and reset operations [34].

V. FIELD TEST RESULTS

In this section, the performance of the right/left error state models is evaluated using pre-collected field test data. Specially, the left error model is used in the INS/GPS integration and the right error model is used in the INS/Odometer integration. For comparison, the traditional INS mechanization (1) is used for INS calculation. With error state definition

$$\delta \mathbf{x} = \begin{bmatrix} \varphi_r & \delta \mathbf{v}^e & \delta \mathbf{p}^e & \boldsymbol{\varepsilon}^b & \nabla^b \end{bmatrix}^T \quad (47)$$

its corresponding error state model is given by

$$\dot{\delta \mathbf{x}} = \mathbf{F} \delta \mathbf{x} + \mathbf{G} \begin{bmatrix} \boldsymbol{\eta}_g^b \\ \boldsymbol{\eta}_a^b \end{bmatrix} \quad (48a)$$

where

$$\mathbf{F} = \begin{bmatrix} -(\boldsymbol{\omega}_{ie}^e \times) & \mathbf{0}_{3 \times 3} & \mathbf{0}_{3 \times 3} & -\tilde{\mathbf{C}}_b^e & \mathbf{0}_{3 \times 3} \\ (\tilde{\mathbf{C}}_b^e \tilde{\mathbf{f}}^b \times) & -2(\boldsymbol{\omega}_{ie}^e \times) & \mathbf{0}_{3 \times 3} & \mathbf{0}_{3 \times 3} & \tilde{\mathbf{C}}_b^e \\ \mathbf{0}_{3 \times 3} & \mathbf{I}_{3 \times 3} & \mathbf{0}_{3 \times 3} & \mathbf{0}_{3 \times 3} & \mathbf{0}_{3 \times 3} \\ \mathbf{0}_{3 \times 3} & \mathbf{0}_{3 \times 3} & \mathbf{0}_{3 \times 3} & \mathbf{0}_{3 \times 3} & \mathbf{0}_{3 \times 3} \\ \mathbf{0}_{3 \times 3} & \mathbf{0}_{3 \times 3} & \mathbf{0}_{3 \times 3} & \mathbf{0}_{3 \times 3} & \mathbf{0}_{3 \times 3} \end{bmatrix} \quad (48b)$$

$$\mathbf{G} = \begin{bmatrix} -\tilde{\mathbf{C}}_b^e & \mathbf{0}_{3 \times 3} \\ \mathbf{0}_{3 \times 3} & \tilde{\mathbf{C}}_b^e \\ \mathbf{0}_{3 \times 3} & \mathbf{0}_{3 \times 3} \\ \mathbf{0}_{3 \times 3} & \mathbf{0}_{3 \times 3} \\ \mathbf{0}_{3 \times 3} & \mathbf{0}_{3 \times 3} \end{bmatrix} \quad (48c)$$

A. INS/GPS Integration

A car-mounted test is carried out for algorithms evaluation. In this experiment, the reference attitude is provided by a POS, which is equipped with a triad of gyroscopes (drift $0.01^\circ/h$) and accelerometers (bias $20\mu g$). The data of an intermediate-grade fiber optic INS with a triad of gyroscopes (drift $0.3^\circ/h$) and accelerometers (bias $20mg$) is collected for algorithms evaluation. The INS sampling rate is 200Hz and the GPS sampling rate is 1Hz. The velocity and position provided by GPS are used as measurements. The length of the collected data is about 850s and the test trajectory is shown in Fig. 1. The integration algorithm making use of INS calculation model (4) and left error model (30) is denoted as LSE-KF and the integration algorithm making use of INS calculation model (1) and error model (48) is denoted as SO-KF.



Fig. 1. Test trajectory for INS/GPS integration

Firstly, the initial attitude error is set as $[1^\circ \ 1^\circ \ 3^\circ]^T$ and the initial velocity and position are provided by GPS directly. The attitude results by the two methods are shown in Fig. 2-4, respectively. It is shown that there is no obvious difference between the two methods. In [21], it is pointed out that making use of the global state independent model can cope with the inconsistency problem caused by false-observability in field of SLAM and VINS. However, for INS/GPS integration, such inconsistency problem is not so obvious, because the heading angle in INS/GPS integration can also be observable. The non-observable state may be the inertial sensors' drift bias. However, for both SO-KF and LSE-KF, the drift bias has not been feedback into the INS calculation. That is to say, the drift bias is estimated in an open-loop manner and the attitude, velocity and position are estimated in close-loop manner. Therefore, the inertial sensors' drift bias will not affect the attitude, velocity and position estimate. The reason for open-loop estimation of inertial sensors' drift bias is that the inertial sensors' drift bias cannot be estimated so well within short time period. The inertial sensors' drift bias estimates by the two methods are shown in Fig. 5 and 6, respectively. It is shown that only the accelerometer bias converges. The gyroscope drift has not been estimated so well. Meanwhile, From Fig. 5 and 6 we can also see that the two methods perform quite similarly.

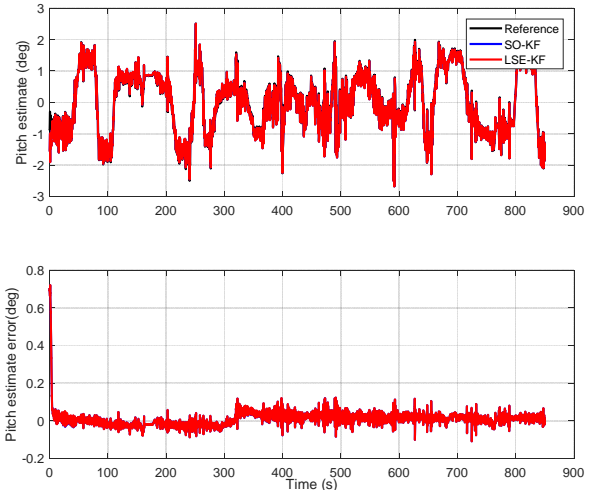


Fig. 2. Pitch angle estimate results in INS/GPS integration with small misalignment

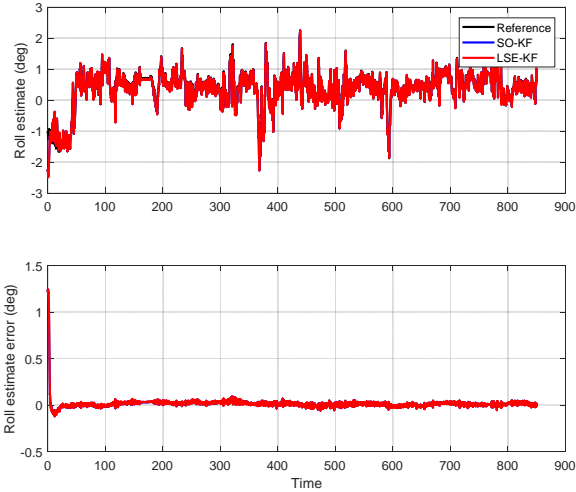


Fig. 3. Roll angle estimate results in INS/GPS integration with small misalignment

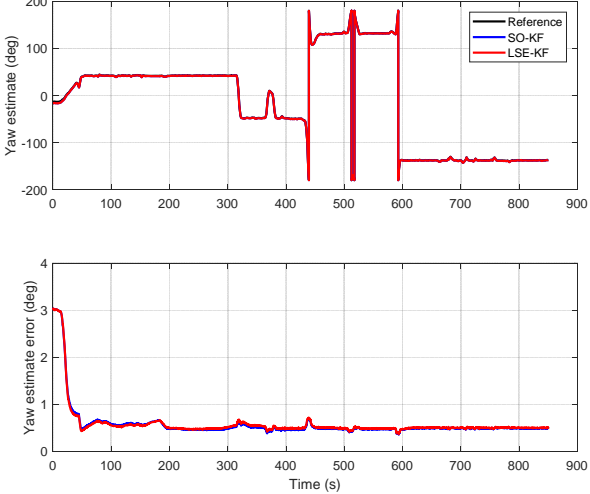


Fig. 4. Yaw angle estimate results in INS/GPS integration with small misalignment

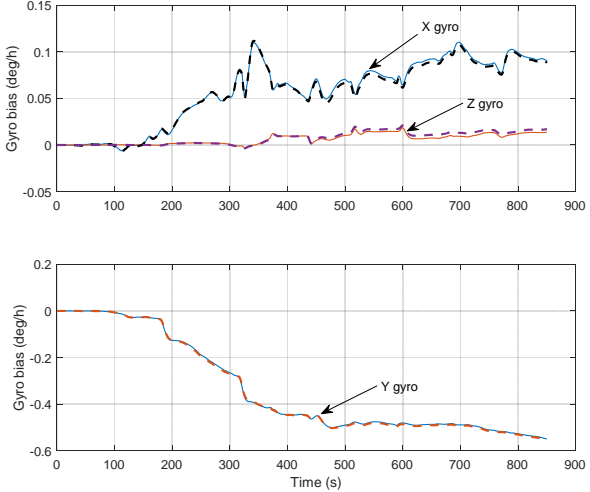


Fig. 5. Gyroscope bias estimate results in INS/GPS integration

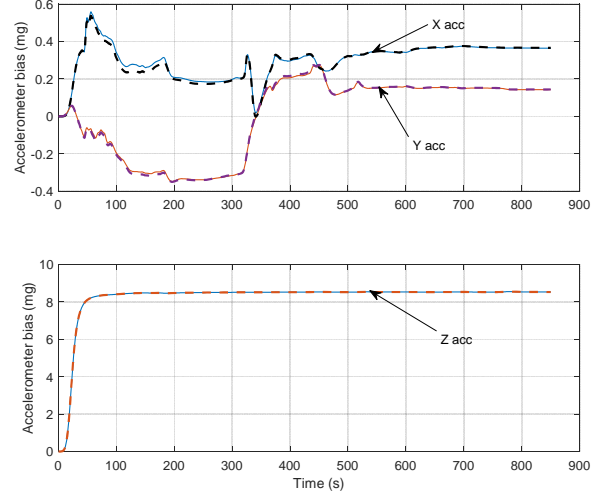


Fig. 6. Accelerometer bias estimate results in INS/GPS integration

According to the above test results analysis, we can know that the advantage of the model has not been exploited since the false-observability in INS/GPS integration is not so obvious. However, another advantage of the left error model (30) is that the nonlinear group error η , can be exactly recovered from the linear error $[\varphi_l^T \quad \mathbf{d}\bar{v}_l^T \quad \mathbf{d}\bar{p}_l^T]^T$. In other word, the linear model (30) can also be applied in case with very large initial attitude error. With this consideration, the initial attitude error is set as $[60^\circ \quad 60^\circ \quad 160^\circ]^T$. The attitude results by the two methods are shown in Fig. 7-9, respectively. The superiority of LSE-KF over SO-KF can now be obvious obtained. LSE-KF can outperform SO-KF in terms of both convergent speed and steady-state accuracy. Such superiority is just derived from the log-linearity of the left error model (30).

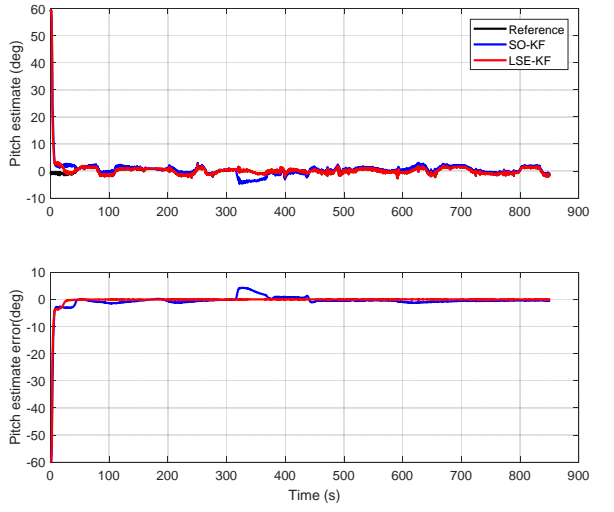


Fig. 7. Pitch angle estimate results in INS/GPS integration with large misalignment

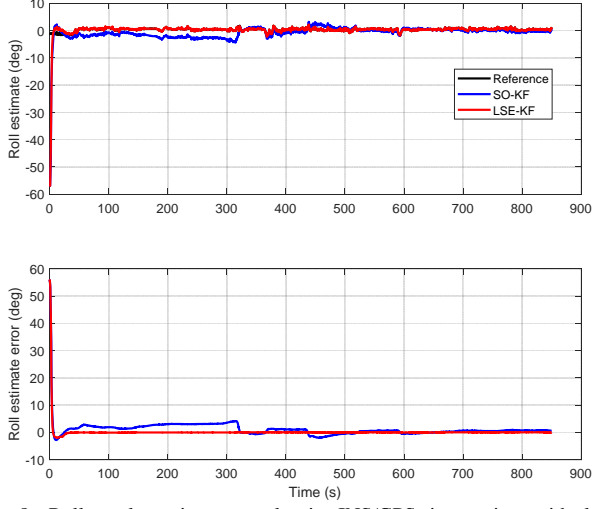


Fig. 8. Roll angle estimate results in INS/GPS integration with large misalignment

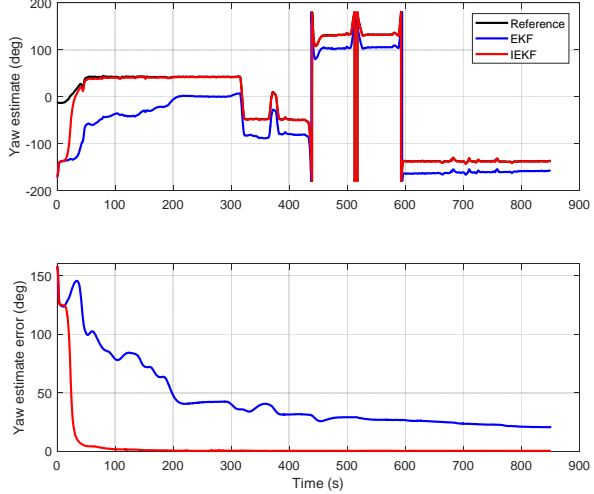


Fig. 9. Yaw angle estimate results in INS/GPS integration with large misalignment

B. INS/Odometer Integration

In this section, the INS/Odometer integration is used to further evaluate the $\mathbb{SE}_2(3)$ based error model. It has been pointed out that, the Odometer measurement is more like right-invariant measurement. Therefore, the right error model (19) is applied. The integration algorithm making use of INS calculation model (4) and right error model (19) is denoted as RSE-KF. The test data was collected from a car-mounted experiment. On the experiment platform there is a navigation grade INS which contains three ring laser gyroscopes with drift of $0.007^\circ/h$ and three quartz accelerometers with bias of $30\mu g$. Besides the INS, the experiment platform also contains a GPS receiver and Odometer. The GPS can provide velocity with precision of about $0.1m/s$ and position with precision of about $10m$ at frequency $1Hz$. The Odometer can provide body velocity with precision of about $\pm 0.5\%$ of its speed at frequency $125Hz$. The results of INS/GPS integration are used as reference. The experiment trajectory is shown in Fig. 10 and the field tests last about 3500 seconds with the distance about $46km$.



Fig. 10. Field tests with the distance about $46km$

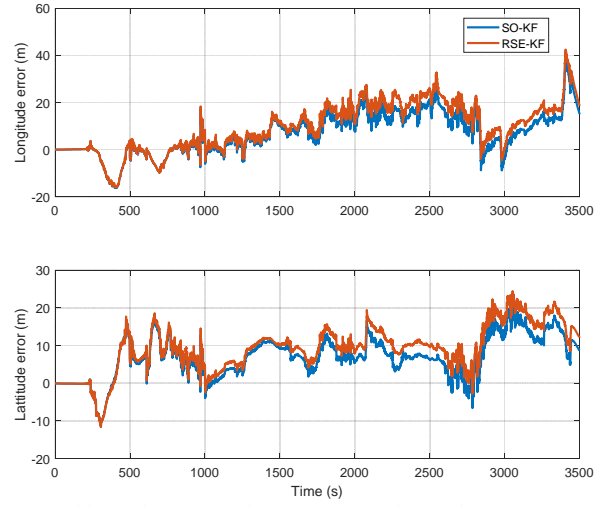


Fig. 11. Position estimate errors in INS/Odometer integration

For both SO-KF and RSE-KF, the initial attitude, velocity and position are all set with the reference values. The latitude and longitude errors by SO-KF and RSE-KF are shown in Fig. 11. It is shown that RSE-KF performs a little worse than SO-KF and the position errors are accumulated with time. This is because that for INS/Odometer integration, the position is non-observable. It is shown in (40) that there is position information in the measurement transition matrix, which will therefore affect the integration performance. In contrast, for the error state definition (47), the linearized measurement function is given by

$$\mathbf{y} = \tilde{\mathbf{v}}^e - \tilde{\mathbf{C}}_b^e \mathbf{v}^b = -(\tilde{\mathbf{v}}^e \times) \boldsymbol{\varphi}_r + \boldsymbol{\delta} \mathbf{v}^e \quad (49)$$

Based on the observability analysis, the position estimate accuracy of INS/Odometer integration is mainly affected by the yaw angle estimate accuracy [35, 36]. As can be seen from the yaw angels estimate results in Fig. 14 that, there are frequent movements in yaw direction, which can improve the corresponding estimate accuracy. The attitude estimate results by the two methods are shown in Fig. 12-14, respectively. The pitch and roll angles estimate results by the two methods are almost the same. Interestingly, the yaw angle estimate result by RSE-KF is a little better than SO-KF, however, the corresponding difference is very slight. Therefore, in this field test, the slight difference in the position estimate errors between the two models is mainly caused by the position related transition matrix in (40). If the test trajectory is straight and it can be expected that false-observability problem caused by yaw

angle estimate will affect the integration performance with model (48). That is to say, the superiority of RSE-KF may be expected in such situation.

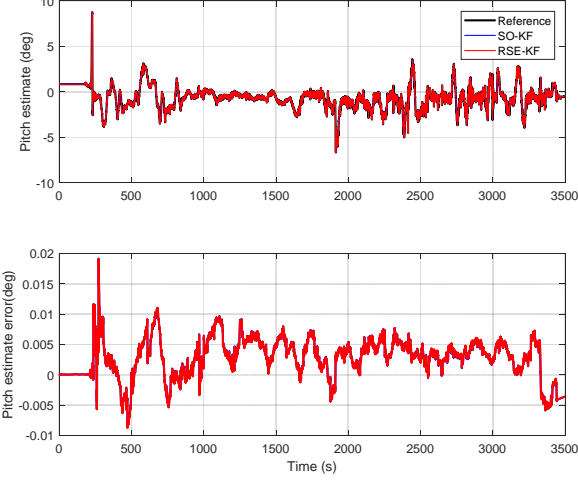


Fig. 12. Pitch angle estimate results in INS/Odometer integration with small misalignment

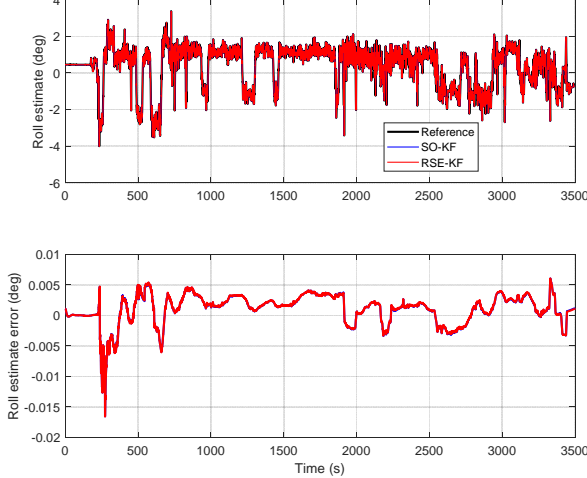


Fig. 13. Roll angle estimate results in INS/Odometer integration with small misalignment

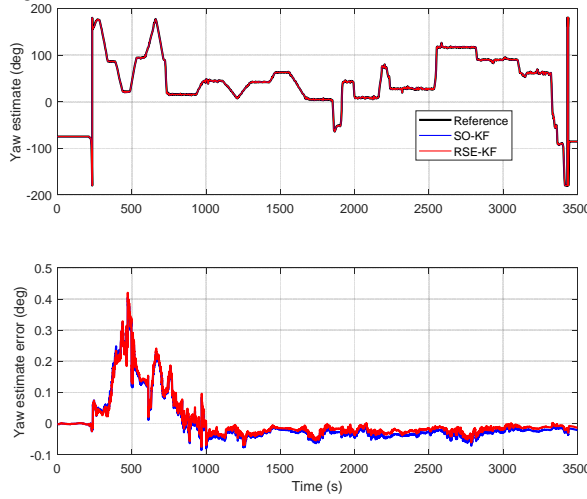


Fig. 14. Yaw angle estimate results in INS/Odometer integration with small misalignment

Another advantage of the $\mathcal{SE}_2(3)$ based model is its ability to handle the large initial misalignment due to its log-linearity.

Therefore, we would also like to check this striking property for INS/Odometer integration. With this consideration, a 600s dynamic data segment is used to evaluate the two models with large initial misalignments. The trajectory of the selected data segment is marked with yellow color in Fig. 10. The initial attitude error is set as $[30^\circ \ 30^\circ \ 60^\circ]^T$. The initial position is set directly using the reference position. The initial velocity is assumed to be zero, which is because that only the body frame velocity can be measured in this application situation. The attitude results by the two methods are shown in Fig.15-17, respectively. It is shown that RSE-KF performs quite better than SO-KF. Such superiority is due to the log-linearity of the attitude, velocity and position error equations in (19b). However, with the right error definition, the measurement transition matrix is not totally trajectory independent, as shown in (40). Therefore, the state-space model (19) and (40) cannot handle extreme large initial misalignments. Actually, we have also carried out the test with initial attitude error $[60^\circ \ 60^\circ \ 160^\circ]^T$ and both RSE-KF and SO-KF cannot converge.

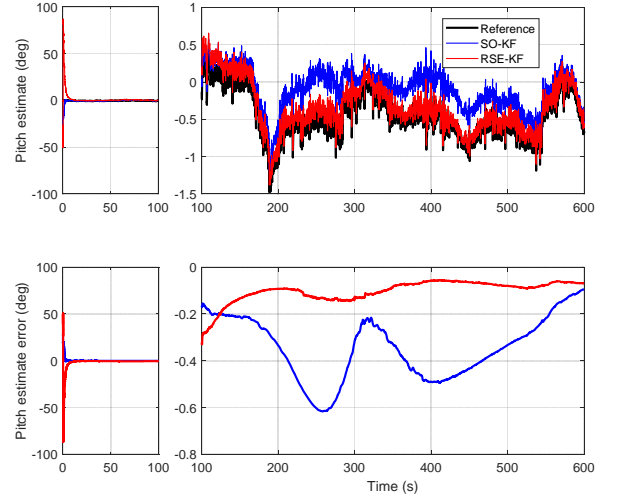


Fig. 15. Pitch angle estimate results in INS/Odometer integration with large misalignment

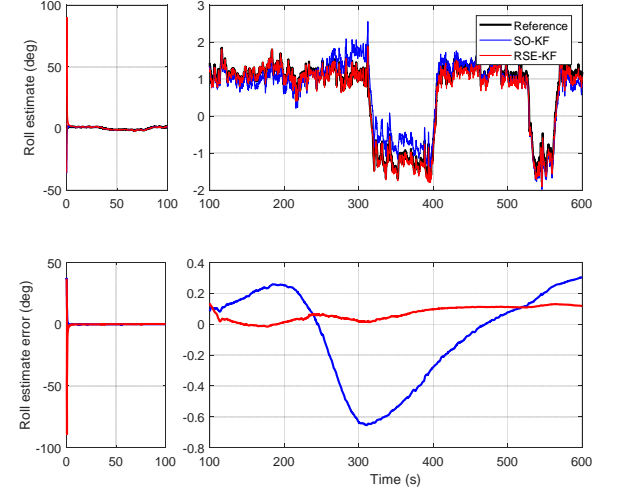


Fig. 16. Roll angle estimate results in INS/Odometer integration with large misalignment

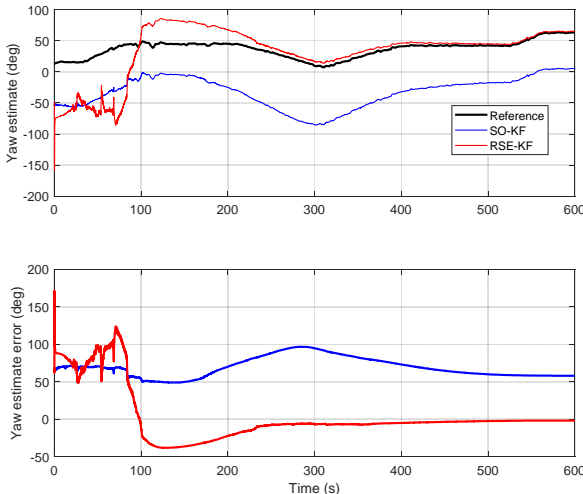


Fig. 17. Yaw angle estimate results in INS/Odometer integration with large misalignment

VI. CONCLUSION

In this paper, the error state models are derived corresponding to a transformed INS mechanization in ECEF. Since the transformed INS mechanization satisfies a *group affine* property with group state on $\mathbb{SE}_2(3)$, the resultant right and left error state models are trajectory independent. Then the error state models are applied in INS/GPS and INS/Odometer integration. It is shown that the advantage of remedying filtering inconsistency by the trajectory-independent error state models has not been brought into play for the two applications. This is because that the false-observability problem of certain state element is not obvious in the two applications. However, another advantage of the trajectory-independent error state models is their log-linearity, which is very suitable for attitude initialization with arbitrary misalignments. For INS/GPS integration, with left error definition, both the process model and measurement model are trajectory independent. Therefore, such linear state space model can still work quite well with even extreme large misalignments. For INS/Odometer integration, however, the measurement model is not totally trajectory independent. The corresponding state space model can only relax the initial attitude accuracy requirement to a certain extent. The experimental study in this paper also indicates that the $\mathbb{SE}_2(3)$ formulation is not essentially superior over $\mathbb{SO}(3)$. How to select the state formulation is dependent on the applications scenarios.

ACKNOWLEDGMENT

The authors would like to thank Prof. Gongmin Yan from Northwestern Polytechnical University for providing the INS/Odometer integration test data.

REFERENCES

- [1] Q. Fu, Y. Liu, Z. Liu, S. Li and B. Guan, "High-Accuracy SINS/LDV Integration for Long-Distance Land Navigation," *IEEE/ASME Transactions on Mechatronics*, vol. 23, no. 6, pp. 2952-2962, Dec. 2018.
- [2] M. Wang, W. Wu, X. He, Y. Li and X. Pan, "Consistent ST-EKF for Long Distance Land Vehicle Navigation Based on SINS/OD Integration," *IEEE Transactions on Vehicular Technology*, vol. 68, no. 11, pp. 10525-10534, Nov. 2019.
- [3] J. Georgy, T. Karamat, U. Iqbal and A. Noureldin, "Enhanced MEMSIMU/odometer/GPS integration using mixture particle filter," *GPS Solut*, vol. 15, pp. 239-252, 2011.
- [4] D. Kang, C. Jang and F. C. Park, "Unscented Kalman Filtering for Simultaneous Estimation of Attitude and Gyroscope Bias," *IEEE/ASME Transactions on Mechatronics*, vol. 24, no. 1, pp. 350-360, Feb. 2019.
- [5] L. Chang, F. Zha and F. Qin, "Indirect Kalman Filtering based Attitude Estimation for Low-cost Attitude and Heading Reference Systems," *IEEE/ASME Transactions on Mechatronics*, vol. 22, no. 4, pp. 1850-1858, 2017.
- [6] J. Wang, T. Zhang, B. Jin, Y. Zhu, and J. Tong, "Student's t-Based Robust Kalman Filter for a SINS/USBL Integration Navigation Strategy," *IEEE Sensors Journal*, vol. 20, no. 10, pp. 5540-5553, 2020.
- [7] T. Bailey, J. Nieto, J. Guivant, M. Stevens, and E. Nebot, "Consistency of the EKF-SLAM algorithm," in *Proc. Int. Conf. Intell. Robots Syst.*, Oct. 2006, pp. 3562-3568.
- [8] G. P. Huang, A. I. Mourikis, and S. I. Roumeliotis, "Observability-based rules for designing consistent EKF SLAM estimators," *The International Journal of Robotics Research*, vol. 29, no. 5, pp. 502-528, Apr. 2010.
- [9] J. A Hesch, D. G. Kottas, S. L. Bowman and S. I. Roumeliotis, "Camera-imu-based localization: Observability and consistency improvement," *The International Journal of Robotics Research*, vol. 33, no. 1, pp. 182-201, 2014.
- [10] G. Huang, M. Kaess and J. J. Leonard, "Towards consistent visual-inertial navigation," In *2014 IEEE International Conference on Robotics and Automation (ICRA)*, 2014, pp. 4926-4933.
- [11] F. N. Li, and L. B. Chang, "MEKF with Navigation Frame Attitude Error Parameterization for INS/GPS," *IEEE Sensors Journal*, vol. 20, no. 3, pp. 1536-1549, 2020.
- [12] M. Li, and A. I. Mourikis, "Improving the Accuracy of EKF-Based Visual-Inertial Odometry," in *Proceedings of the IEEE International Conference on Robotics and Automation*, pp. 828-835, 2012.
- [13] M. Li, and A. I. Mourikis, "High-precision, consistent EKF-based visual-inertial odometry," *The International Journal of Robotics Research*, vol. 32, no. 6, pp. 690-711, 2013.
- [14] H. Gui, and A. H. J. de Ruiter, "Quaternion Invariant Extended Kalman Filtering for Spacecraft Attitude Estimation," *Journal of Guidance, Control, and Dynamics*, vol. 41, no. 4, pp. 863-878, 2018.
- [15] M. S. Wang, W. Q. Wu, P. Y. Zhou and X. F. He, "State transformation extended Kalman filter for GPS/SINS tightly coupled integration," *GPS Solutions*, vol. 22, no. 4, pp. 1-12, 2018.
- [16] M. S. Wang, W. Q. Wu, X. F. He, Y. Li and X. F. Pan, "Consistent ST-EKF for Long Distance Land Vehicle Navigation Based on SINS/OD Integration," *IEEE Transactions on Vehicular Technology*, vol. 68, no. 11, pp. 10525-10534, 2019.
- [17] S. Heo and C. Park, "Consistent EKF-based visual-inertial odometry on matrix Lie group," *IEEE Sensors Journal*, vol. 18, no. 9, pp. 3780-3788, May 2018.
- [18] S. Heo, J. H. Jung, and C. G. Park, "Consistent EKF-based visual inertial navigation using points and lines," *IEEE Sensors Journal*, vol. 18, no. 18, pp. 7638-7649, Sep. 2018.
- [19] T. Zhang, K. Wu, J. Song, S. Huang, and G. Dissanayake, "Convergence and consistency analysis for a 3-D invariant-EKF SLAM," *IEEE Robot. Autom. Lett.*, vol. 2, no. 2, pp. 733-740, Apr. 2017.
- [20] M. Brossard, A. Barrau, and S. Bonnabel, "Exploiting Symmetries to Design EKFs With Consistency Properties for Navigation and SLAM," *IEEE Sensors Journal*, vol. 19, no. 4, pp. 1572-1579, Sep. 2019.
- [21] A. Barrau and S. Bonnabel, "An EKF-SLAM algorithm with consistency properties," arXiv:1510.06263, 2015.
- [22] A. Barrau, Non-linear state error based extended Kalman filters with applications to navigation. PhD thesis, Mines Paristech, 2015.
- [23] A. Barrau and S. Bonnabel, "The Invariant Extended Kalman Filter as a Stable Observer," *IEEE Transaction on Automatic Control*, vol. 62, no. 4, pp. 1797-1812, 2017.
- [24] A. Barrau and S. Bonnabel, "A Mathematical Framework for IMU Error Propagation with Applications to Preintegration," in *Proceedings of the IEEE International Conference on Robotics and Automation*, 2020.
- [25] M. Brossard, A. Barrau, P. Chauchat and S. Bonnabel, "Associating Uncertainty to Extended Poses for on Lie Group IMU Preintegration with Rotating Earth," arXiv:2007.14097v1, 2020.
- [26] R. Hartley, M. Ghaffari, R. M. Eustice and J. W. Grizzle, "Contact-Aided Invariant Extended Kalman Filtering for Robot State Estimation," *The*

International Journal of Robotics Research, 2020.

[27] Q. W. Fu, Q. Zhou, G. M. Yan, S. H. Li and F. Wu, "Unified all-earth navigation mechanization and virtual polar region verification," *IEEE Transactions on Instrumentation and Measurement*, 10.1109/TIM.2020.3041819, 2020.

[28] Y. Wu, C. He and G. Liu, "On inertial navigation and attitude initialization in polar areas," *Satellite Navigation*, 10.1186/s43020-019-0002-4, 2020.

[29] Q. W. Fu, F. Wu, S. H. Li and Y. Liu "In-motion Alignment for a Velocity-aided SINS with Latitude Uncertainty," *IEEE/ASME Transactions on Mechatronics*, vol. 25, no. 6, pp. 2893-2903, 2020.

[30] Y. L. Huang, Y. G. Zhang, and L. B. Chang, "A new fast in-motion coarse alignment method for GPS-aided low-cost SINS," *IEEE/ASME Transactions on Mechatronics*, vol. 23, no. 3, pp. 1303–1313, Jul 2018.

[31] X. Cui, C. B. Mei, Y. Y. Qin, G. M. Yan, and Q. W. Fu, "In-motion Alignment for Low-cost SINS/GPS under Random Misalignment Angles," *The Journal of Navigation*, vol. 70, pp. 1224–1240, 2017

[32] X. Xu, Z. T. Guo, Y. Q. Yao and T. Zhang, "Robust Initial Alignment for SINS/DVL Based on Reconstructed Observation Vectors," *IEEE/ASME Transactions on Mechatronics*, vol. 25, no. 3, pp. 1659–1667, Jul 2020.

[33] F. L. Markley, "Lessons Learned," *Journal of Astronautical Sciences*, vol. 57, no. 1–2, pp. 3–29, 2009.

[34] J. L. Crassidis, and F. L. Markley, "Unscented filtering for spacecraft attitude estimation," *Journal of Guidance, Control, and Dynamics*, vol. 26, no. 4, pp. 536–542, 2003.

[35] Y. Wu, "Versatile land navigation using inertial sensors and odometry: Self-calibration, in-motion alignment and positioning," in *Proc. Inertial Sensors Syst.-Symp. Gyro Technol. (ISS-SGT)*, pp. 1-19, Karlsruhe, Germany, 16-17, September. 2014.

[36] Y. Wu, C. Goodall, N. El-sheemy, "Self-calibration for IMU/Odometer Land Navigation: Simulation and Test Results," in *Proceedings of the ION International Technical Meeting*, San Diego, CA, USA, 25–27 January 2010.